Aerosol Science and Technology

ISSN: (Print) (Online) Journal homepage: www.tandfonline.com/journals/uast20

Measurement of 100 nm monodisperse particles by four Accurate methods: Traceability and uncertainty

George W. Mulholland, Kaleb J. Duelge, Vincent A. Hackley, Natalia Farkas, John A. Kramar, Michael R. Zachariah, Keiji Takahata, Hiromu Sakurai & Kensei Ehara

To cite this article: George W. Mulholland, Kaleb J. Duelge, Vincent A. Hackley, Natalia Farkas, John A. Kramar, Michael R. Zachariah, Keiji Takahata, Hiromu Sakurai & Kensei Ehara (2024) Measurement of 100 nm monodisperse particles by four Accurate methods: Traceability and uncertainty, Aerosol Science and Technology, 58:3, 323-333, DOI: 10.1080/02786826.2024.2310548

To link to this article: https://doi.org/10.1080/02786826.2024.2310548

Published online: 12 Feb 2024.

AEROSOL SCIENCE AND TECHNOLOGY
2024, VOL. 58, NO. 3, 323–333
https://doi.org/10.1080/02786826.2024.2310548

Measurement of 100 nm monodisperse particles by four Accurate methods: Traceability and uncertainty

George W. Mulholland[a,b], Kaleb J. Duelge[a,b], Vincent A. Hackley[a], Natalia Farkas[a,c], John A. Kramar[a], Michael R. Zachariah[d], Keiji Takahata[e], Hiromu Sakurai[e], and Kensei Ehara[e]

[a]Materials Research Laboratory, National Institute of Standards and Technology, Gaithersburg, Maryland, USA; [b]Chemical and BioMolecular Engineering, University of Maryland, College Park, Maryland, USA; [c]Building and Fire Sciences, US Forest Service, Forest Products Laboratory, Madison, Wisconsin, USA; [d]Chemical Engineering and Materials Science, University of California, Riverside, California, USA; [e]National Institute of Advanced Industrial Science and Technology, Umezono Tsukuba, Japan

ABSTRACT

Accurate measurements of particle diameter are necessary for quantitative characterization of key aerosol properties including the Cunningham slip correction factor, charging probability, diffusion coefficient, coagulation coefficient, and optical properties. In this study, we use four techniques to measure the diameter of nominal 100 nm reference spheres having a distributional standard deviation of less than 2 nm. The instruments used are a differential mobility analyzer (DMA), atomic force microscopy (AFM), scanning electron microscopy (SEM), and an electrical-gravitational aerosol balance (EAB). All four measurements are traceable to SI units at National Institute of Standards and Technology (NIST) or at National Institute of Advanced Industrial Science and Technology (AIST). This study includes quantitative estimates of the measurement uncertainty for each technique. It finds that the measured average particle diameter is within 3% for all the methods, with at least some overlap in all the estimated uncertainties using a 95% confidence interval. Nevertheless, the difference between the EAB results and the other methods may become significant as they are separately intended to be used in the manner described here for the traceable certification of future nanoscale particle size standards. Possible reasons for the differences are incorrect or inadequate accounting for surface residue for aerosol measurements, adhesion-force distortion for the AFM measurements, e-beam shrinkage for the SEM measurements, slip correction uncertainty for the DMA, and work function variability of the electrodes for the EAB.

ARTICLE HISTORY
Received 9 October 2023
Accepted 8 January 2024

EDITOR
Jason Olfert

Introduction

Accurate size standards are critical to fundamental studies in aerosol science. These include the measurement of the Cunningham slip correction factor, charging probability, diffusion coefficient, coagulation rate, and optical properties.

An important aspect of a certification standard is traceability, where the parameter of interest is linked to the relevant International System of Units (SI) unit. A NIST standard reference material (SRM) is an artifact that has its property values certified by a technically valid procedure that is traceable to the SI. One approach for establishing traceability for nanoparticles has been relating the diameter measurement to the wavelength of light of various laser sources of accurately known wavelength. This is the approach used for the AFM and SEM measurements. For the EAB method, the voltmeter, gauge blocks, and hydrometer used in the determination of the certified values were calibrated traceable to the System of Units (SI). For the DMA, the traceability is *via* the voltage measurements and the NIST SRM 1963a calibration particles. In principle, the specific traceability pathway should not matter and various measurement techniques using a variety of traceable sources should result in the same value within the limits of measurement uncertainty. Good agreement has been demonstrated between nanoscale traceability methods based on the wavelength of light and crystal lattice length (Dai et al. 2016). We further investigate this idea by comparing measurements of the same nanoparticle sample by four techniques with three different traceability approaches.

CONTACT George W. Mulholland georgewm@umd.edu Chemical and BioMolecular Engineering, University of Maryland, 4418 Stadium Drive, College Park, MD 20742-3035, USA.

It is also critical that the measurement uncertainty of the standard be small so that it does not limit the uncertainty of the measurements that are based on it. The uncertainty analysis includes those affects that can be calculated by standard statistical tools (Type A uncertainty) as well as those based on scientific judgment (Type B uncertainty) (Taylor and Kuyatt 1994). The combined uncertainty is computed from these components.

Near-monodisperse standards avoid the complication of different methods tending to be biased in the average diameter they measure because of responding differently to the size distribution. A notable example is dynamic light scattering, where the lack of reliable measurements of the size distribution renders it impossible to justifiably convert the directly measured intensity-weighted harmonic mean to a number-weighted arithmetic mean (also called the number average), which is the most common central value measurand used for particle size method comparisons. For a monodisperse standard, all the central values collapse to one value independent of Pythagorean mean and weighting. This at least provides a reliable common reference point for calibrating disparate methods without resorting to method-dependent measurands (Farkas and Kramar 2021).

Nanoparticle size standards are an essential need for instrument calibration, which corrects measured value to true value; and for instrument validation, which verifies measured value within the desired range of true value. The use of the same standards—samples from the same lot—can help promote coherence between different techniques and increase reproducibility of experimental results. One example (Wiedensohler et al. 2012) is the standardized technical set-up for mobility particle size spectrometers, which includes particle size calibration using monodisperse spherical polystyrene latex (PSL) particles with accurately known particle diameters, in the framework of the European Supersites for Atmospheric Aerosol Research/Aerosols, Clouds, and Trace Gases Research Infrastructure Network.

There have been a number of interlaboratory studies involving state of the art instruments of the same type being used to measure the same particle sample. This provides important information on the reproducibility of the measurements. These studies include: six laboratories (Montoro Bustos et al. 2015) using single-particle inductively-coupled plasma – mass spectrometry (spICP-MS) to measure the size of the NIST gold nanoparticle Reference Materials 8012 and 8013 (nominal 30 nm and 60 nm diameter); fourteen national metrology institutes worldwide (Koenders et al. 2003) participating in a comparison of five step height standards in the range of 7 nm to 800 nm, which were measured with AFMs; eight laboratories using transmission electron microscopy (Rice et al. 2013) to measure the size distribution of nominal 30 nm NIST SRM 8012; and 11 laboratories measuring the light absorption cross section of a soot simulate using photoacoustic spectroscopy (Zangmeister and Radney 2018). While these studies are important in their own right, they do not necessarily provide a measure of accuracy and traceability of the particle size measurements.

There has not been a published intercomparison of traceable measurement techniques for the same sample by laboratories providing primary calibration standards for nanometer size spherical particles. The intention of this paper is to provide a first step in correcting this situation by providing a snapshot of where the aerosol community is in terms of the accurate measurement of 100 nm spherical PSL particles based on work at two national metrology institutes. It involves four measurements methods: one from the National Institute of Advanced Industrial Science and Technology (AIST) in Japan and three from the Materials Measurement Laboratory and the Physical Measurement Laboratory at NIST. This effort originated from AIST providing a narrowly distributed PSL particle suspension to NIST after completing measurements with their improved electro-gravitational aerosol balance (EAB). This PSL particle suspension has a coefficient of variation (CV) less than 2%—CV being the ratio of the standard deviation of the size distribution to the average diameter.

Differential mobility analysis (DMA), atomic force microscopy (AFM), and scanning electron microscopy (SEM) were used at NIST to measure the number average diameter, D_n—also called the count mean diameter—of the AIST-provided nominally 100 nm polystyrene PSL particles (JSR SC-010-S—notably the same PSL lot from which the NIST SRM 1963 samples were taken 33 years ago) as shown in Equation (1)

$$D_n = \frac{\sum_{i-1}^{N_B} D_i \frac{\Delta N_i}{\Delta D_i} \Delta D_i}{\sum_{i-1}^{N_B} \Delta N_i} = \frac{\sum_{i-1}^{N} D_i n_D(D_i) \Delta D_i}{N_t} = \sum_{i=1}^{N_B} D_i p(D_i) \Delta D_i \quad (1)$$

where N_i is the cumulative number distribution and ΔN_i is the number concentration of particles in bin i (with diameters between D_i and D_{i+1}), i is the bin index, N_B is the total number of bins, $n_D(D_i)$ is the number distribution, $p(D_i)$ is the frequency function, ΔD_i is the width of the ith bin, and N_t is the total number concentration of particles. The above definition is for an aerosol where N_t is the total number

concentration of the aerosol with units of inverse volume. For the microscopy, N_t is the total number of particles sized with no units. These are nearly spherical particles with a relatively monodisperse and symmetrical diameter distribution. The measurements listed above were compared to measurements by the EAB of the same sample (Takahata et al. 2020). The DMA measurements were calibrated with a size standard traceable to the wavelength of light through previous light scattering measurements. The AFM and SEM measurements were calibrated with size artifacts traceable to the wavelength of light through interferometry. The EAB is considered a primary measurement technique with a quantitative uncertainty budget based on the uncertainties of the component measured quantities.

This study summarizes the major uncertainties associated with each method for the measurement of the number average diameter. The detailed uncertainty analyses are given in the references. For the DMA, the major uncertainties and the calibration are discussed by Duelge et al. (2022). The certification measurements for SRM 1963a, which was used in the DMA calibration, are discussed in Mulholland et al. (2006) and the uncertainty in the slip correction factor used in the DMA measurements is discussed in Kim et al. (2005). For the EAB, a detailed uncertainty analysis was given by Ehara, Takahata, and Koike (2006b) and was later extended by Takahata et al. (2020) to include the effect of the electrode work function. The theoretical basis for the EAB is given by Ehara, Takahata, and Koike (2006a). Dagata et al. (2016) characterized the effect of the PSL sphere – mica substrate deformation on the uncertainty in the sphere diameter for the AFM. Montoro Bustos et al. (2018) quantified the uncertainty in the diameter obtained using SEM for 30 and 60 nm gold particles. The uncertainty analysis for measuring PSL spheres with the SEM is an ongoing study.

The measured size and uncertainty for each technique is described, and possible reasons for the differences between results are discussed. For each measurement type there are multiple components affecting the uncertainty such as the voltage in the case of the DMA and EAB and the particle image boundary thresholding for the SEM. The component uncertainties are summed into a combined uncertainty, $u_c(D)$, by the law of propagation of uncertainty, often referred to as the "root-sum-of-squares" (RSS) (Taylor and Kuyatt 1994),

$$u_c^2(D) = \sum_{i-1}\left[\frac{\partial D}{\partial x_i}\right]^2 u^2(x_i) = \sum_{i-1}\left[c_i u(x_i)\right]^2 = \sum_{i=1} u_i^2(D) \quad (2)$$

where it is assumed that the variables x_i are uncorrelated. The partial derivatives are evaluated based on an analytic relationship or numerically. Below, the component uncertainties of the diameter, $u_i(D)$, are given. Ultimately the results are presented as the expanded uncertainty, which is an interval over which there is a specified probability that the measurand (true diameter) is in the interval. This expanded uncertainty is computed using a coverage factor, $k = 2$, taken to represent an approximate 95% confidence interval, multiplied by the combined standard uncertainty.

Materials

Nominally 100 nm PSL particles JSR SC-010-S, nominally 100 nm PSL particles NIST SRM 1963a, and 18.2 MΩ·cm filtered deionized water (Model 2121AL, Aqua Solutions, Jasper, GA, USA) were used. Ammonium acetate (>99.99%), used in the electrospray aerosol generator, was purchased from Sigma Aldrich (St. Louis, MO, USA). The identification of any commercial product or trade name does not imply endorsement or recommendation by the National Institute of Standards and Technology.

Measurement methods and uncertainties

Differential mobility analysis

The DMA measurements were made using an electrospray atomizer - differential mobility analyzer (DMA) - condensation particle counter (CPC) system. The long DMA (Model 3081, TSI, Shoreview, MN, USA) was used with a sheath flow of 20 L·min^{-1} and an aerosol flow rate of 1 L·min^{-1} air. Prior to measurement by the DMA, the particles were bath sonicated for 5 min, diluted by a factor of 10 using 18.2 MΩ·cm deionized water, passed through a 0.2 μm filter, and diluted again by a factor of 10 in 154 mg·L^{-1} ammonium acetate at pH 8. Particles were electrosprayed (Model 3480, TSI), mobility selected, and then counted by a butanol CPC (Model 3776, TSI) operating at 1.5 L·min^{-1}. A tee fitting was placed at the entrance of the CPC with an attached HEPA filter to compensate the mismatch between the aerosol flow and the CPC flow. The DMA was used in step voltage mode, single pass using custom LabVIEW code (0.5 nm step and 30 s dwell time). The CPC counts were averaged for 20 s followed by a 10 s pause after changing voltage. After the 20-min scan, the voltage was manually returned to the peak position and it was verified that the concentration at the peak voltage had

changed by no more the 10%. Low drift over the measurement time is important. The temperature and pressure of the sheath flow were measured immediately after exiting the DMA by a flow meter (Series 4000, Model 4043H, TSI) with a stated accuracy of 1.0 K and 0.2 kPa. The power supply was calibrated with a voltage divider (Model HUD-100-1, Spellman, Hauppauge, NY, USA) and a voltage meter (Model 34401 A, Agilent Technologies, Santa Clara, CA, USA). The flow rate was calibrated with a DryCal (Model Defender 530). Duelge et al. (2022) derive the equation used here for relating the number size distribution to the CPC value at selected voltage, charging probability, the slip correction, and the ratio of aerosol flow to the sheath flow.

Measurements of SRM 1963a with a certified peak diameter of 101.8 nm ± 1.1 nm (95% confidence interval) were used for calibrating the DMA. The estimated values of the number average diameter and the standard deviation of the size distribution are 101.1 and 3.0 nm with a CV of 3%. These are not certified values but estimated values based on the frequency distribution measurements shown in Figure 1. The size distribution is slightly skewed toward smaller particle sizes with the peak diameter about 0.7 nm larger than the number average diameter.

If the measured peak diameter for the calibration particles does not agree with the certified value, the data are post-processed by changing the sheath flow value in the equation relating the diameter, voltage, and sheath flow (Equation (3), Duelge et al. (2022) by a few percent. The peak diameter is recomputed. This is an iterative process typically requiring 3 to 4 iterations. The peak diameter is computed by fitting the region near the peak (upper 40% to 50% with 11 to 13 data points) to a cubic polynomial and then setting the derivative of the function equal to zero. This approach is similar to that described by Duelge et al. (2022). The modified flow rate is used in analyzing the DMA data for an unknown sample.

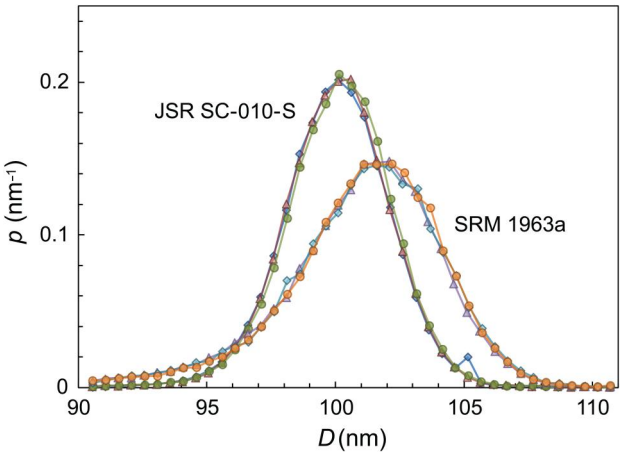

Figure 1. Comparison of DMA frequency function measurements of JSR SC-010-S and calibrant SRM 1963a (certified value of 101.8 nm ± 1.1 nm). The number average diameters for the three repeats for the JSR SC-010-S particles are 100.1, 100.1, and 100.2 nm.

The number of particles counted over the 20-min scan was 2.1×10^5 for JSR SC-010-S and 6.1×10^4 for SRM 1963a. The background CPC concentration for the filtered ammonium acetate solution was about 0.4 cm^{-3} compared to peak concentrations of about 1680 cm^{-3} for JSR SC-010-S and about 530 cm^{-3} for SRM 1963a. The primary uncertainties are the diameter of the calibration standard (standard uncertainty (u_{cs}) = 0.54 nm), repeatability of measurements (u_r = 0.20 nm), mode voltage uncertainty of the unknown particle (u_{VI} = 0.04 nm), mode voltage uncertainty of the calibration particle (u_V = 0.03 nm), and negligible contributions from the slip correction, temperature, and pressure. Note that the quoted uncertainties are the derived diameter uncertainties arising from these various factors (see Equation (2)). The combined standard uncertainty computed by the RSS is 0.58 nm and the expanded uncertainty, with $k=2$, is 1.2 nm.

Repeat measurements of the frequency functions of the calibrant particle and the JSR SC-010-S particles are displayed in Figure 1. The data runs are fit with a normal distribution from which the number average diameters and CVs are determined and averaged to be 100.2 nm ± 1.2 nm and 2.0%, respectively.

Atomic force microscopy

Well-dispersed individual JSR SC-010-S nanoparticles were attached to a poly-L-lysine-coated mica substrate by leaving a 50-µL droplet of the sample on the substrate for several minutes, but without allowing the droplet to dry. To remove unattached particles, the substrate was rinsed and immersed in deionized water followed by drying with air. AFM images of the samples were acquired under ambient conditions with a Veeco MultiMode AFM and Nanoscope IV controller. Nanoscope version 6 software was used for data acquisition, and Nanoscope V software was used for analysis. Particle size by AFM is reported as height after background flattening and adhesion-deformation correction. The AFM was calibrated using a set of step height standards, which had been previously calibrated with the NIST Calibrated Atomic Force Microscope (Dixson et al. 1999). Their height values and uncertainties ($k=2$) are 6.6 nm ± 0.1 nm, 20.1 nm ± 0.3 nm, 67.7 nm ± 0.4 nm, 290.4 nm ± 0.9, and 779.7 nm ± 2.7 nm.

The major components contributing to the measurement uncertainty of the particle height arise from repeatability of the measurements ($u_r = 0.7$ nm), particle-substrate deformation ($u_{def} = 0.7$ nm), peak-to-valley background flatness ($u_f = 0.3$ nm), and calibration ($u_{cal} = 0.3$ nm). The combined standard uncertainty is estimated *via* RSS. The expanded uncertainty calculated at the 95% confidence interval ($k = 2$) for the AFM number average height measurements of JSR SC-010-S is 2.3 nm.

The height frequency function obtained from individual particle measurements by AFM is shown in Figure 2 along with a representative AFM topography image. The AFM height data are corrected for calibration and for the estimated 3.2 nm particle-substrate attachment flattening deformation (Dagata et al. 2016). The data is fit with a normal distribution from which the number average height and CV are determined to be 99.3 nm ± 2.3 nm and 1.7%, respectively.

The distributional quality of the JSR SC-010-S particles was also qualitatively assessed by AFM raft measurements. A 5-µL, dilute droplet of the sample was allowed to dry on a freshly-cleaved mica substrate. The particles raft well, forming close-packed arrays as shown in Figure 3, and exhibit high distributional uniformity, i.e., only a small percentage of the particles are visually significantly smaller or larger than the number average diameter.

Scanning electron microscopy

Well-dispersed individual nanoparticles were attached to a poly-L-lysine-coated silicon substrate in the same manner as the samples prepared for AFM on mica. The images were collected with an FEI Helios dual-beam SEM. Image analysis was done with custom ImageJ routines, using the maximum entropy threshold to set the particle boundary. Particle size by SEM is reported as the diameter of a circular-equivalent area. The magnification of the SEM was calibrated using a 100 nm VLSI grating pitch standard, which had been previously calibrated with NIST's Calibrated Atomic Force Microscope. Its pitch value is 99.94 nm with an expanded uncertainty of 0.06 nm ($k = 2$).

The major components contributing to the measurement uncertainty of the number average circular-area-equivalent diameter arise from the repeatability of measurements ($u_r = 0.5$ nm), determination of the

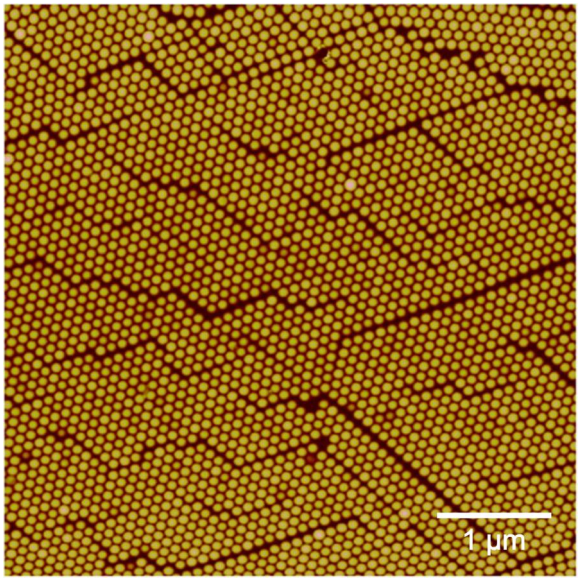

Figure 3. AFM raft images of JSR SC-010-S.

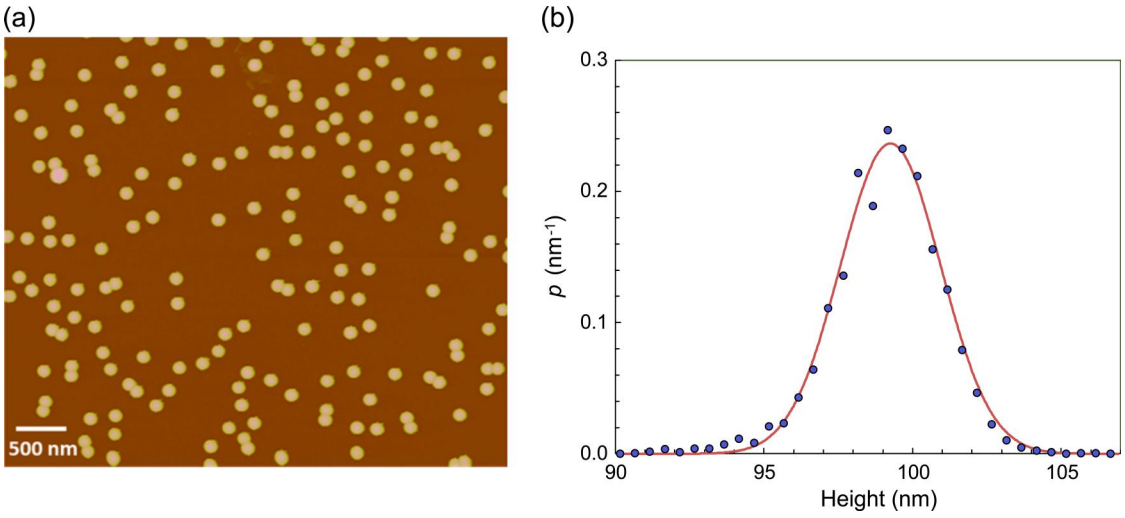

Figure 2. (a) Representative AFM topography image and (b) height frequency function of JSR SC-010-S. The AFM height data is corrected for particle-substrate deformation. 3257 particles were analyzed. The points correpond to the binned height frequency function for a 0.5 nm bin width. The curve is a normal distribution fit to the full, unbinned data set.

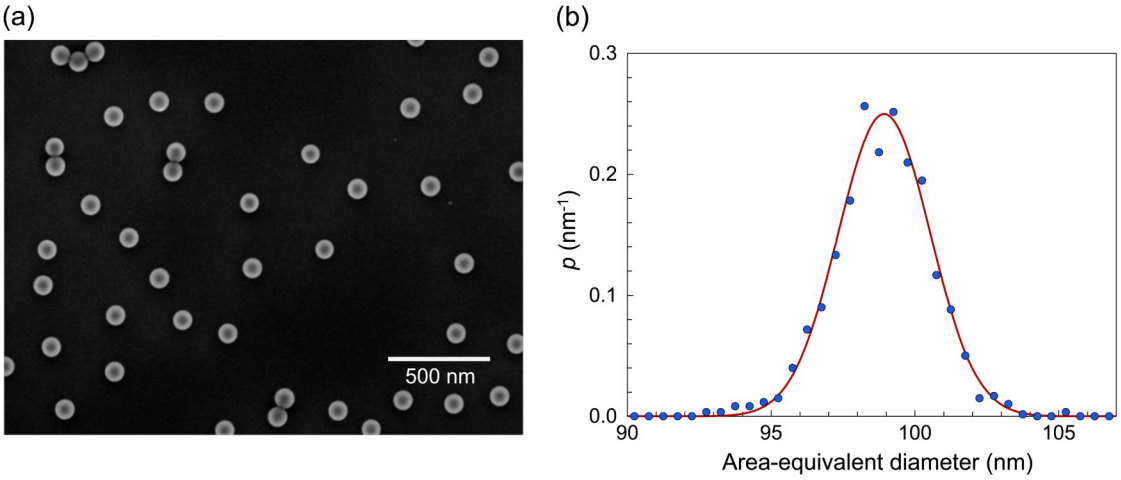

Figure 4. (a) Representative SEM image and (b) area-equivalent diameter frequency function of JSR SC-010-S. The points correspond to the binned height frequency function for a 0.5 nm bin width. 1201 particles were analyzed. The curve is a normal distribution fit to the full, unbinned data set.

particle boundary by thresholding (u_b = 0.8 nm), e-beam spot size (u_{ss} = 0.3 nm), digitization of the particle projection area (u_d = 0.4 nm), stage drift (u_{sd} = 0.3 nm), and e-beam-induced shrinkage (u_s = 1.5 nm). The combined standard uncertainty is estimated *via* RSS. The expanded uncertainty calculated at the 95% confidence interval ($k = 2$) for the SEM number average diameter measurements of JSR SC-010-S is 3.7 nm.

The area-equivalent-diameter frequency function obtained from individual particle measurements by SEM is shown in Figure 4 along with a representative SEM image. The data is fit with a normal distribution from which the number-average area-equivalent diameter of JSR SC-010-S by SEM is 98.9 nm ± 3.7 nm and the CV is 1.6%.

Electro-gravitational aerosol balance

The EAB is a unique, large scale Millikan-cell type instrument that measures the loss of particles between parallel electrodes with various applied voltages to determine the number-average mass of aerosolized particles (Ehara et al. 2006a). Figure 5a shows a top and side view of the electrodes, the gauge block spacers, and the 12 annular holes for the aerosol or clean air to enter the cell and to exit to either the particle counter or to exhaust. The basic measurement quantity is the survival function—which is defined as the ratio of the number of particles left suspended after a certain holding time has elapsed relative to the initial number of particles—as a function of the particle mass.

The key physical quantity for the EAB is the terminal velocity v of the particle computed from a force balance of the gravitational force, electrical force, and drag force acting on the particle.

$$v = \frac{C_c(D)}{3\pi\eta D}\left[\frac{eV}{H} - \left(1 - \frac{\rho_{air}}{\rho_p}\right)\frac{\pi}{6} g \rho_p D^3\right] \tag{3}$$

where η is the viscosity, e the charge of an electron, H the distance between the electrodes, ρ_p and ρ_{air} the density of the particle and of air, g the acceleration of gravity, and $C_c(D)$ the Cunningham slip correction factor. The equation for the survival rate as a function of the terminal velocity v ignoring diffusion is given by

$$\begin{aligned} S(V,D) &= 1 - |v| t_h / H \quad \text{if } t_h \\ &\leq H/v \qquad = 0 \text{ otherwise} \end{aligned} \tag{4}$$

where t_h is the holding time. When the electrical and gravitational forces are equal, the velocity is 0 and the survival rate is 1. Or if the distance traveled by a given particle size over the hold time were $\frac{1}{2}$ H either in the positive or negative z direction, then half of those particles would have reached one of the electrode surfaces and the predicted value of the survival function for that size would be one half.

Figure 5b shows the survival rate spectra of JSR SC-010-S obtained from the four sets of EAB measurements needed in order to evaluate and correct for the work function imbalance between the opposing electrode surfaces of EAB cell (Takahata et al. 2020). In Figure 5b, for example, the symbol I (A/p/B) is used to represent the configuration I, positively charged particles are introduce in the EAB cell with electrodes A and B used as the upper and lower electrodes, respectively; for more details, see Takahata et al. 2020. The holding time is chosen to be 7 h.

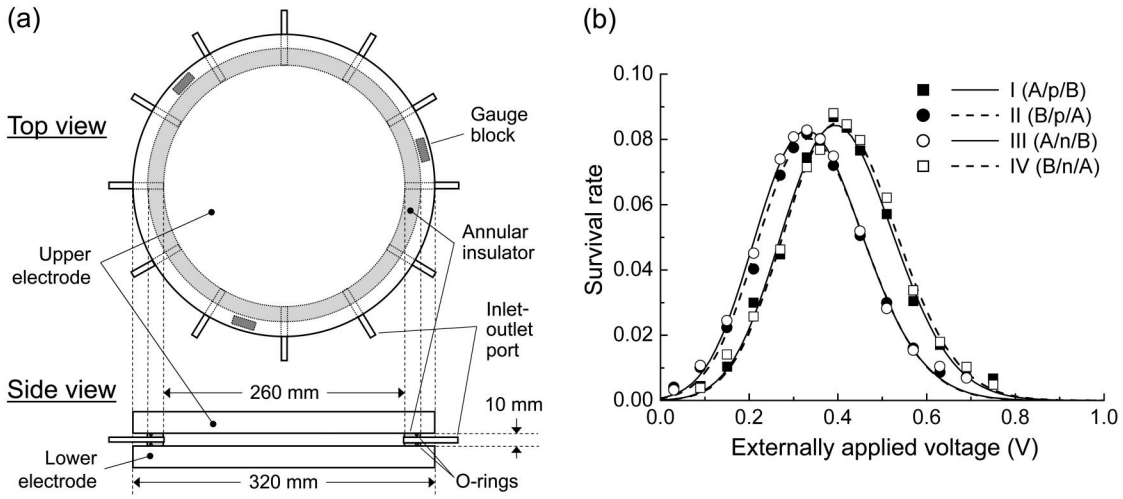

Figure 5. (a) Electrodes used for the EAB experiment. (b) EAB spectra of the 100 nm PSL particles (JSR SC-010-S) obtained from four sets of EAB measurements (see also Table 1). (Reproduced with permission of the American Association for Aerosol Research, Takahata, Sakurai, and Ehara 2020.)

Table 1. Summary of the uncertainty components for EAB for the 100 nm PSL particles JSR SC-010-S.

Remarks	Standard uncertainty $u(S_i)$	$u_A(m)/m$	$\frac{u_A(D_n)}{D_n}$	$\frac{u_B(D_n)}{D_n}$	Combined relative standard uncertainty
Configuration I (A/p/B)	3.0×10^{-3}	1.0×10^{-2}	3.4×10^{-3}	7.6×10^{-4}	3.5×10^{-3}
Average of 4 configurations	–	5.3×10^{-3}	1.8×10^{-3}	7.6×10^{-4}	1.9×10^{-3}

The survival rate $S_f(V_i)$ for a polydisperse aerosol is given by the following average:

$$S_f(V_i) = \frac{c}{\sqrt{2\pi}\sigma}\int \exp\left[\frac{-(D-D_n)^2}{2\sigma^2}\right] S(V_i, D)dD. \quad (5)$$

$S_f(V_i)$ is fitted to the measured survival rates $S(V_i)$ by adjusting the number average diameter D_n, the standard deviation of the size distribution σ, and a scaling constant c, using the least squares method to minimize the sum of the squares SS,

$$SS = \sum_{i=1}^{n} \left(S(V_i) - S_f(V_i)\right)^2 \quad (6)$$

where V_i refers to the ith voltage setting.

Table 1 summarizes the uncertainty associated with the residual fitting error in the survival rate spectrum $u(S_i)$, the mass uncertainty $u(m)$, and the combined uncertainty of D_n. With three adjustment parameters in the fitting, the number of degrees of freedom of Equation (5) is $n - 3$. Hence, we obtain

$$u(S_i) = \sqrt{SS/(n-3)}. \quad (7)$$

The procedure for evaluation of uncertainty of the Type A components of $u_A(m)$ is described in Ehara et al. 2006b, where m is the particle mass. The values for $u_A(m)$ are given in Table 1.

From the relationship between the diameter and the mass of a spherical particle and from Equation (2), the following equation is obtained between the uncertainty in the diameter and the uncertainties of the mass and of the particle density:

$$\left(\frac{u(D)}{D}\right)^2 = \left(\frac{u(m)}{3m}\right)^2 + \left(\frac{u(\rho)}{3\rho}\right)^2 \quad (8)$$

This equation is applied to calculating the uncertainty in the particle diameter. The major component of the Type B uncertainty is the density, which has a value of 1.0632 g/cm^3 and a standard uncertainty of 0.0022 g/cm^3. The resulting number average diameter and expanded uncertainty are 101.71 and 0.39 nm, respectively.

Comparisons

Figure 6 and Table 2 compare measurement results for the number average diameter and the expanded uncertainty of the JSR SC-010-S by the four techniques. For AFM, SEM and DMA, the normal distribution fit as well as the D_n of the full data set are presented. D_n differs by at most 0.2% from the normal distribution fit, and is smaller due to the slight tailing of the distribution toward smaller particle sizes. An advantage of measuring JSR SC-010-S is that the measurands from the different techniques are expected to be nearly identical. DMA measures mobility, AFM measures height, SEM measures area, and EAB measures mass, but all of the number average diameters

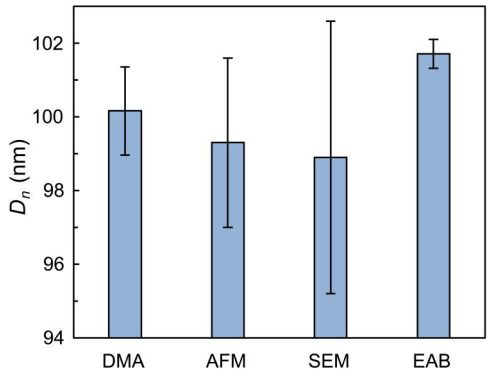

Figure 6. Number average diameter and expanded uncertainty for four size measurement techniques.

Table 2. Number average diameter, expanded uncertainty, and CV of the distribution for JSR SC-010-S using four size measurement techniques.

	Normal distribution fit		All data including outliers*	Expanded uncertainty
Technique	D (nm)	CV (%)	D_n (nm)	(2 σ) (nm)
DMA	100.2	2.0	100.1	1.2
AFM	99.3	1.7	99.1	2.3
SEM	98.9	1.6	98.8	3.7
EAB	101.71	N/A		0.39

*For the DMA, the number average is limited to the range of particles between 90 nm and 110 nm.

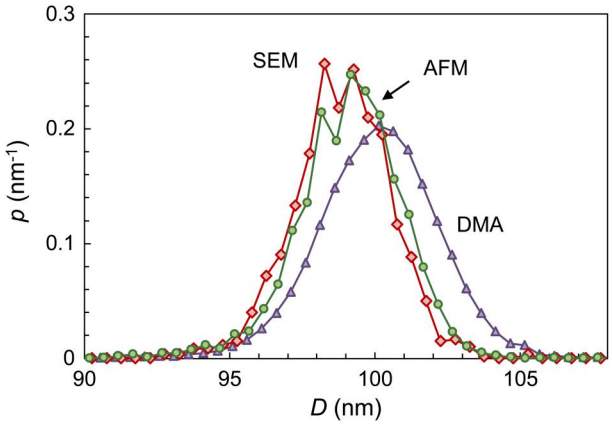

Figure 7. Comparison of the frequency functions for AFM, SEM, and DMA.

derived from these different properties are expected to be nearly the same, as the particles are essentially spherical with a narrow size distribution and known density. There are two noteworthy observations from these results. First the smallness of the uncertainty in the EAB relative to the other techniques. Secondly, the uncertainty range for each measurement overlaps at least slightly with that of the other methods.

The diameter frequency function obtained by the AFM and SEM are narrower than the DMA results as seen in Figure 7. The EAB does not provide a measurement of the frequency function. The CV is about 20% smaller for the microscopy measurements than the DMA measurement (1.7% AFM, 1.6% SEM, and 2.0% DMA). It is thought that the microscopy results are closer to the true width of the frequency function. However, the statistics are much better for the DMA than the microscopy with about 2.1×10^5 particles sized by DMA versus 1202 by SEM and 3257 by AFM.

Discussion

Different traceability paths were used for the different measurements in this comparison. The DMA measurements are traceable to the wavelength of light of a He-Ne laser (632.9908 nm, with standard uncertainty of 1.5×10^{-6}, Stone 2009) which was used to determine the number average diameter of SRM 1690 by light scattering measurements of the particle suspension (Mulholland et al. 1985). SRM 1690 was used as a calibration particle for DMA measurements of SRM 1963, nominally 100 nm PSL particles. Finally, due to aggregation, SRM 1963 was eventually replaced with SRM 1963a, also nominally 100 nm PSL particles. SRM 1963 was used as a calibration particle for the certification DMA measurements of SRM 1963a and SRM 1964 (nominally 60 nm PSL particles) (Mulholland et al. 2006). SRM 1963a is used as the traceable calibration particle in the current study. The AFM and SEM measurements are traceable to the calibrated AFM at NIST which uses laser interferometers having laser frequencies traceable to an iodine-stabilized He-Ne laser. The calibrated AFM is a carefully designed metrology grade instrument that is used to certify size standards such as the height and pitch standards used to calibrate the AFM and SEM measurements presented here (Dixson et al. 1999).

The EAB is used as a primary measurement technique that does not require a calibration standard of the same quantity as the measurand. In addition, the force balance theory is straightforward, and this method has a much smaller estimated uncertainty. A detailed uncertainty analysis for the EAB was made, and comparison measurements were made of several size standards certified by different measurements (Ehara et al. 2006a, 2006b). Good agreement was determined for seven PSL particles ranging from 100 nm to 1000 nm, including a variety of traceable standards such as SRM 1963, SRM 1691, and SRM 1690. For 5 of 7 samples for which density was measured, the density ranged from 1.055 g/cm^3 to 1.065 g/cm^3. Due to the mass being proportional to the cube of the diameter,

the relative uncertainty in the diameter resulting from the density uncertainty is only one third of the relative density uncertainty.

Repeat measurements by the EAB over several years had shown some drift in the measured diameter of JSR SC-010-S. It was shown that the measured work functions of the electrodes had a significant—and potentially temporally changing—influence on the measurement due to electrode degradation (Takahata et al. 2020). For the 100 nm PSL measurements, when including the work function correction, the expanded uncertainty decreased from 0.66 nm to 0.39 nm, with the residual fitting errors in the survival function having the largest contribution to the uncertainty. The new measured value for JSR SC-010-S is 101.71 nm ± 0.39 nm.

The uncertainty of the EAB method is at least 3 times smaller than the other measurements and the other values are significantly outside the uncertainty range of the EAB. This is an intriguing situation worthy of more attention. Inadequate compensation of the work function could be a potential factor. Measurements of the particle diameter for 300 nm PSL particles have been made by the EAB and because the maximum-survival voltage for these is about a factor of 30 larger than it is for the 100 nm particles, the work function effect was negligible. Measurements of this same lot of 300 nm PSL particles using the other techniques described above could help resolve the differences between the various measurement methods.

There are also some lingering potential bias and uncertainty questions with the other techniques. In the case of the SEM, there is a known issue of the shrinkage of the polystyrene spheres in the electron beam. In AFM, the sphericity of the particles is affected by surface forces when depositing the particles on a substrate during sample preparation thus decreasing the measured height; there could also be tip-particle deformation during imaging, although steps were taken to avoid this (Dagata et al. 2016). Corrections are made for these effects; however, these issues require further study for decreasing the uncertainty. For the DMA, it is possible that the uncertainty associated with the Cunningham slip correction of the sphere is larger than the current estimate.

The SEM and AFM measurements involve particles on poly-L-lysine-coated substrates, while the DMA and EAB measure the aerosolized particles after droplet evaporation. Perhaps the different environments affect the thickness of a coating on the surface of the spheres. In one study of 100 nm PSL particles the estimated coating thickness was about 0.01 nm (Ehara et al. 2006b) and in a second study of 100 nm spheres the estimated thickness was 0.11 nm (Mulholland et al. 2006). It is also possible that there is a surfactant coating that remains bound to the particle despite dilution in deionized and filtered water.

The EAB is being used to certify size standards by the National Metrology Institute of Japan (NMIJ), while the AFM and SEM methods described here are being used to certify the next generation size standards at NIST. The differences revealed here are expected to also be true for these future standards, with the NIST number average size values being slightly smaller than the NMIJ values and the uncertainty ranges likely overlapping. This may complicate future international comparisons as the results may vary depending on the source of calibration standard. Support from organizations focusing on particle measurements is needed for the continuation of primary particle calibration standards, which are currently not available from NIST for 100 nm particle diameter.

It is also important that these calibration particles be measured by other widely used basic techniques such as transmission electron microscopy (Rice et al. 2013), small angle x-ray scattering (Wong et al. 2020), and dynamic light scattering (Farkas and Kramar 2021). Two of these methods allow one to measure the particle diameter of the spheres in the liquid phase.

Conclusions

The total range in the number average diameters for the four measurements of JSR SC-010-S (100 nm monodisperse polystyrene spheres) is 3% of the average of the averages and there is some overlap in the uncertainty ranges between all four methods. For many applications, the use of this standard—or a replacement since the current standard is no longer available—would enhance the quality of size distribution measurements for spherical aerosols and colloids. However, it is notable that the 95% confidence interval for the EAB method, which has the lowest uncertainty, only fully overlaps with the SEM uncertainty range. The uncertainty ranges of each of the other three methods are within 0.1 nm of overlapping the number average diameter of the other two though the uncertainty bounds are wide relative to the EAB results. This difference between EAB results and the other methods may become significant as they are intended to be used separately in the manner described here for the certification of future nanoscale particle size standards. Potential sources of the

differences include incorrect estimates of surface residue for the DMA and EAB, slip correction uncertainty for the DMA measurements, adhesion-force distortion for the AFM measurements, e-beam shrinkage for the SEM measurements, and inadequate compensation for work function variations for the EAB.

Acknowledgement

We acknowledge Kavuri P. Purushotham (NIST) for performing SEM imaging.

Disclosure statement

No potential conflict of interest was reported by the author(s).

Funding

KJD was supported in part by a grant from the National Institute of Standards and Technology, Materials Measurement Science Division [Award No. 70NANB17H057].

ORCID

George W. Mulholland http://orcid.org/0000-0001-7889-3599
Kaleb J. Duelge http://orcid.org/0000-0002-6367-3822
Vincent A. Hackley http://orcid.org/0000-0003-4166-2724
Natalia Farkas http://orcid.org/0000-0002-7102-7345
John A. Kramar http://orcid.org/0000-0001-6038-637X
Keiji Takahata http://orcid.org/0000-0002-2535-3633
Hiromu Sakurai http://orcid.org/0000-0002-0933-2074
Kensei Ehara http://orcid.org/0000-0002-2179-5151

References

Dagata, J. A., N. Farkas, P. Kavuri, A. E. Vladar, C. L. Wu, H. Itoh, and K. Ehara. 2016. Method for measuring the diameter of polystyrene latex reference spheres by atomic force microscopy. Special Publication (NIST SP) 260–185.

Dai, G. L., L. Koenders, J. Fluegge, and H. Bosse. 2016. Two approaches for realizing traceability in nanoscale dimensional metrology. *Opt. Eng.* 55 (9):091407. doi: 10.1117/1.OE.55.9.091407.

Dixson, R., R. Köning, V. W. Tsai, J. Fu, and T. V. Vorburger. 1999. Nanometer-scale dimensional metrology with the NIST calibrated atomic force microscope. *Microsc. Microanal.* 5 (S2):958–9. doi: 10.1017/S1431927600018110.

Duelge, K., G. Mulholland, M. Zachariah, and V. Hackley. 2022. Accurate nanoparticle size determination using electrical mobility measurements in the step and scan modes. *Aerosol Sci. Techno.* 56 (12):1096–113. doi: 10.1080/02786826.2022.2128986.

Ehara, K., K. Takahata, and M. Koike. 2006a. Absolute mass and size measurement of monodisperse particles using a modified Millikan's method: Part I – Theoretical framework of the electro-gravitational aerosol balance. *Aerosol Sci. Technol.* 40 (7):514–20. doi: 10.1080/02786820600714379.

Ehara, K., K. Takahata, and M. Koike. 2006b. Absolute mass and size measurement of monodisperse particles using a modified Millikan's method: Part II – Application of electro-gravitational aerosol balance to polystyrene latex particles of 100 nm to 1 mu m in average diameter. *Aerosol Sci. Technol.* 40 (7):521–35. doi: 10.1080/02786820600714387.

Farkas, N., and J. A. Kramar. 2021. Dynamic light scattering distributions by any means. *J. Nanopart. Res.* 23 (5):120. doi: 10.1007/s11051-021-05220-6.

Kim, J. H., G. W. Mulholland, S. R. Kukuck, and D. Y. H. Pui. 2005. Slip correction measurements of certified PSL nanoparticles using a nanometer differential mobility analyzer (nano-DMA) for Knudsen number from 0.5 to 83. *J. Res. Natl. Inst. Stand. Technol.* 110 (1):31–54. doi: 10.6028/jres.110.005.

Koenders, L., R. Bergmans, J. Garnaes, J. Haycocks, N. Korolev, T. Kurosawa, F. Meli, B. C. Park, G. S. Peng, G. B. Picotto, et al. 2003. Comparison on Nanometrology: Nano 2-Step height. *Metrologia* 40 (1A): 04001. doi: 10.1088/0026-1394/40/1A/04001.

Montoro Bustos, A. R., E. J. Petersen, A. Possolo, and M. R. Winchester. 2015. Post hoc interlaboratory comparison of single particle ICP-MS size measurements of NIST gold nanoparticle reference materials. *Anal. Chem.* 87 (17): 8809–17. doi: 10.1021/acs.analchem.5b01741.

Montoro Bustos, A. R., K. P. Purushotham, A. Possolo, N. Farkas, A. E. Vladár, K. E. Murphy, and M. R. Winchester. 2018. Validation of single particle ICP-MS for routine measurements of nanoparticle size and number size distribution. *Anal. Chem.* 90 (24):14376–86. doi: 10.1021/acs.analchem.8b03871.

Mulholland, G. W., A. W. Hartman, G. G. Hembree, E. Marx, and T. R. Lettieri. 1985. Development of a one-micrometer-diameter particle-size standard reference material. *J Res. Natl. Bur. Stand.* 90 (1):3–26. doi: 10.6028/jres.090.001.

Mulholland, G. W., M. K. Donnelly, C. R. Hagwood, S. R. Kukuck, V. A. Hackley, and D. Y. H. Pui. 2006. Measurement of 100 nm and 60 nm particle standards by differential mobility analysis. *J. Res. Natl. Inst. Stand. Technol.* 111 (4):257–312. doi: 10.6028/jres.111.022.

Rice, S. B., C. Chan, S. C. Brown, P. Eschbach, L. Han, D. S. Ensor, B. Aleksandr, A. B. Stefaniak, J. Bonevich, A. E. Vladár, et al. 2013. Particle size distributions by transmission electron microscopy: An interlaboratory comparison case study. *Metrologia.* 50 (6):663–78. doi: 10.1088/0026-1394/50/6/663.

Stone, J. A. 2009. Uncalibrated helium-neon lasers in length metrology. *NCSL Int. Measure.* 4 (3):52–8. doi: 10.1080/19315775.2009.11721483.

Takahata, K., H. Sakurai, and K. Ehara. 2020. Accurate determination of mass and diameter of monodisperse particles by the electro-gravitational aerosol balance: Correction for the work function imbalance between the electrode surfaces. *Aerosol Sci. Technol.* 54 (12):1386–98. doi: 10.1080/02786826.2020.1787324.

Taylor, B. N., and C. E. Kuyatt. 1994. Guidelines for evaluating and expressing the uncertainty of NIST measurement results. NIST Technical Note 1297 (1994 Edition) National Institute of Standards and Technology.

Wiedensohler, A., W. Birmili, A. Nowak, A. Sonntag, K. Weinhold, M. Merkel, B. Wehner, T. Tuch, S. Pfeifer, M.

Fiebig, et al. 2012. Mobility particle size spectrometers: Harmonization of technical standards and data structure to facilitate high quality long-term observations of atmospheric particle number size distributions. *Atmos. Meas. Tech.* 5 (3):657–85. doi: 10.5194/amt-5-657-2012.

Wong, J. C., L. Xiang, K. H. Ngoi, C. H. Chia, K. S. Jin, and M. Ree. 2020. Quantitative structural analysis of polystyrene nanoparticles using synchrotron x-ray scattering and dynamic light scattering. *Polymers.* 12 (2):477. doi: 10.3390/polym12020477.

Zangmeister, C. D., and J. G. Radney. 2018. NIST interlaboratory study of aerosol absorption measurements using photoacoustic spectroscopy national institute of standards and technology: Gaithersburg, MD, 27 April 2018.